JOURNAL OF SOLID STATE CHEMISTRY 75, 73–89 (1988)

The Solvolytic Disproportionation of Mixed-Valence Compounds

III. Pb_3O_4

Z. C. KANG, LAURA MACHESKY*, H. A. EICK,† AND L. EYRING‡

Department of Chemistry and the Center for Solid State Science, Arizona State University, Tempe, Arizona 85287

Received June 15, 1987, in revised form January 4, 1988

The chemical transformation corresponding to the equation

$$Pb_3O_4(s) + 4H^+(aq) = PbO_2(s) + 2Pb^{2+}(aq) + 2H_2O(l)$$

has been studied chemically but especially by high-resolution electron microscope (HREM) observations on specimens quenched at regular intervals during reaction. It was determined that attack by the acid solution is most rapid along {101} directions with a substantial component along [001]. "PbO" as well as PbO_2 go into solution as Pb^{2+} and water. This requires electrons to be supplied to the reacting surface. As a consequence, a receding (101) edge, free of PbO_2 precipitate, is usually maintained thin by the reaction. The precipitation of PbO_2 occurs as an independent process separated spatially from the dissolution reaction according to the equation

$$Pb^{2+}(aq) + 2H_2O(l) = PbO_2(s) + 4H^+(aq) + 2e^-.$$

This reaction is reversible and the rapid exchange between $Pb^{2+}(aq)$ and PbO_2 promotes simultaneous and continuous recrystallization. This mechanism, elucidated by HREM techniques, is also consistent with the gross chemical kinetic and X-ray studies.

Introduction

Certain homogeneous compounds of mixed-valence cations are selectively leached by a suitable solvent. This leaching process removes into solution only part of the compound. It is to be expected that the mechanism of this process would be highly dependent upon the structures and structural defects of the reactant and product and also, to some extent, on the particular solvent used for leaching. It is desirable to generate plausible atomic-level reaction mechanisms for various categories of these reactions, which we will call "solvolytic disproportionation," to continue a previous usage (*1*). To this end, high-resolution electron microscopy is applied to the study of leached materials, quenched at various stages of the process.

The intermediate oxides of Pr and Tb have been studied by this technique (*2, 3*) with surprising differences in the mechanism even for these very similar oxides. The intermediate oxides of both elements are fluorite related and the product remaining in both cases is the fluorite dioxide.

* Present address: The Johns Hopkins University, Baltimore, MD 21211.

† On sabbatical leave from Department of Chemistry, Michigan State University, East Lansing, MI 48824.

‡ To whom correspondence should be addressed.

0022-4596/88 $3.00

Sixty years ago Bruckner (*4*) observed that when Pb_3O_4 was reacted with acetic acid a lead superoxide acetate was formed. It is known (*5*) that when Pb_3O_4 is leached with dilute mineral acid, PbO_2 remains. However, the process must be quite different than that for the rare earth oxides because structural differences between the reactant and product require a reconstructive change. Pb_3O_4 is tetragonal with $a = 8.815$ and $c = 6.605$ Å (*6–8*) while β-PbO_2 is also tetragonal but with $a = 4.955(3)$ and $c = 3.383(2)$ Å (*9*). Transport phenomena in the solid and solution are different among the various examples, as are the species and reactions occurring at the liquid–solid interface.

No mechanistic studies of the solvolytic disproportionation of Pb_3O_4 have been published although many aspects of its chemistry relative to this process have been characterized. References to some of these studies will be made at the appropriate places below.

Experimental Part

Procedure

The Pb_3O_4 from Baker (1–2334) was heated to constant weight (48 hr) at 475°C and stored in a desiccator over anhydrous $CaSO_4$ until used.

Approximately 100-mg samples of Pb_3O_4 and 25 or 50 ml of dilute nitric acid were placed in 150-ml beakers and stirred constantly. At 30-min intervals the pH and temperature of the contents of each beaker were measured. On these occasions the contents of one of the remaining beakers were filtered (thereby stopping the reaction) and washed with distilled water. The beakers, stirring bars, and glass filtering crucibles containing the remaining Pb_3O_4 and the solid PbO_2 residue were then dried by heating at 110°C to constant weight. This procedure was continued until all the specimens (usually eight) had been weighed.

The progress of the reaction was established by the mass of the residue, determined as described above, and the assumption that only PbO_2 and unreacted Pb_3O_4 remained. A 34.9% recovery corresponds to a completed reaction. The solid residue remaining after each interval was collected and stored in a desiccator for further study by X-ray analysis and by transmission electron microscopy.

Specimens of the original material and of material quenched during reaction were examined by X-ray powder diffractometry. A Rigaku DMax-IIB automatic diffractometer with a curved graphite monochrometer in the diffracted beam was used to collect patterns of diffraction maxima of each sample. CuK_α radiation was used. The raw data were smoothed and the background subtracted using the software provided by the manufacturer. The final output gives numbers to the peaks and prints a table giving 2θ, calculated d-spacing, FWHM, and the relative intensity for each peak. The peaks in the diffractograms were compared to those listed on the relevant ASTM cards to determine the compounds present.

Samples of the original, final, and each quenched intermediate preparation were also taken for examination on the JEOL 200CX and the Philips-400ST electron microscopes. The specimens were dispersed in alcohol by ultrasonic vibration and the dispersion applied to holey carbon films supported on copper microscope grids. Observation was made by well-established techniques (*10*).

Results

X-ray diffraction patterns of powders of the starting, final, and intermediate solid phases were used to monitor the course of the reaction. In Figs. 1a and 1b the diffractograms are shown for the starting and final materials, Pb_3O_4 and β-PbO_2, respectively. The diffraction maxima are in ac-

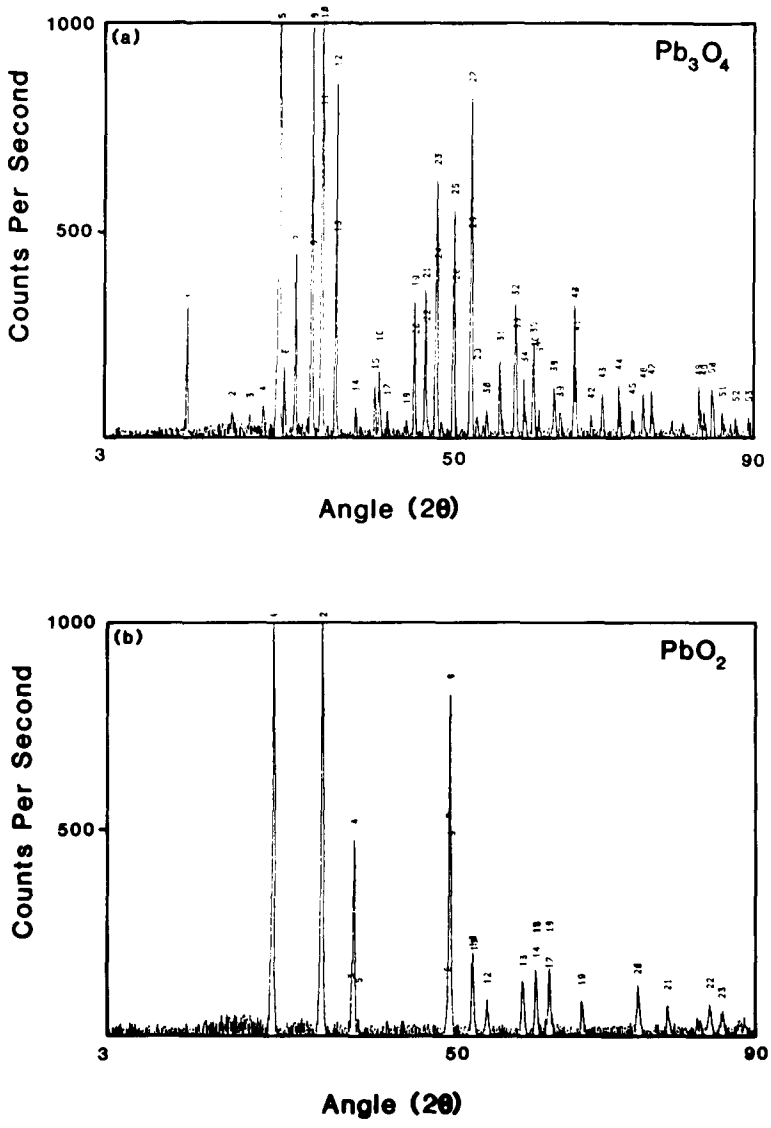

FIG. 1. (a) The X-ray powder diffraction pattern of the starting material, Pb_3O_4. (b) The X-ray powder diffraction pattern of the final reaction product, β-PbO_2.

cord with the literature values in both cases. Diffraction patterns of the solid residue taken after $\frac{1}{2}$, 1, 2, and 4 hr of leaching are shown in Figs. 2a–2d. These can be resolved into an increasing amount of β-PbO_2 in the diminishing reactant, Pb_3O_4. All reflections are accounted for by a combination of these two patterns. The quantitative determination of the relative amounts of Pb_3O_4 and PbO_2 was best determined from the weight of the residue, however.

It was desirable to find a concentration of HNO_3 that would provide an optimum reaction rate. One hundred milligrams of Pb_3O_4 was reacted with 25 ml of 1 *N* HNO_3 and the reaction was found to be over in $\frac{1}{2}$ hr,

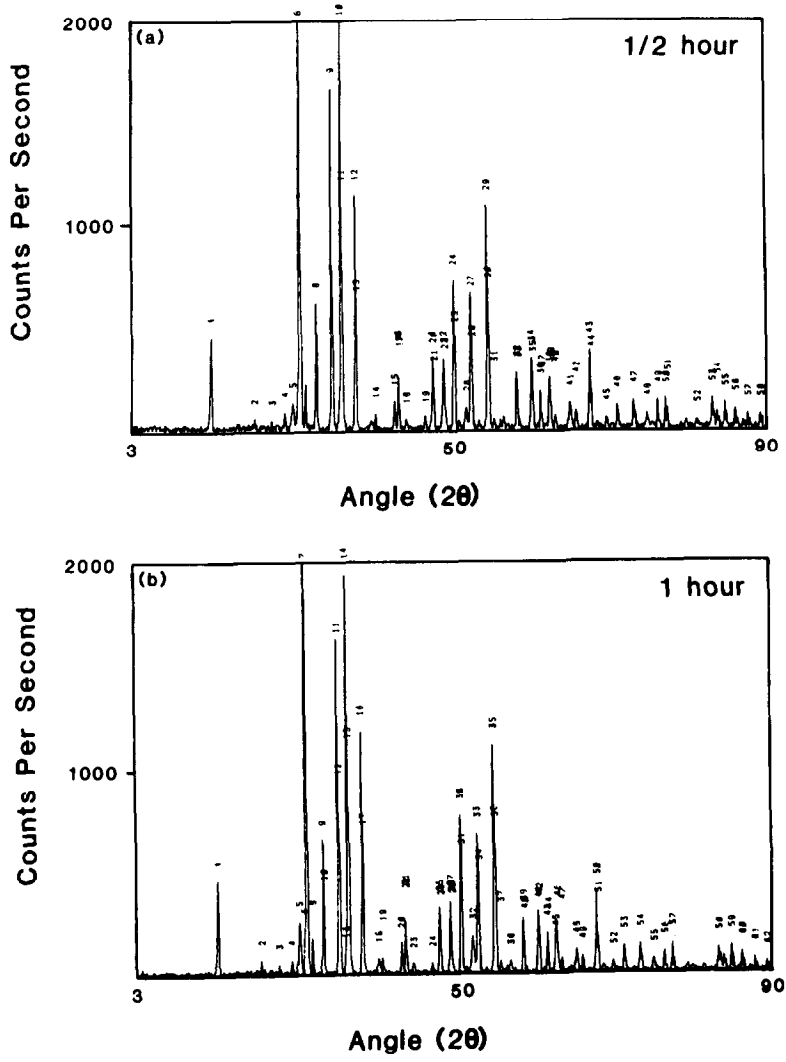

FIG. 2. (a) The X-ray powder diffraction pattern of reaction product after $\frac{1}{2}$ hr showing a weak β-PbO_2 pattern growing in. (b) The X-ray powder diffraction pattern after 1 hr showing increased diffraction maxima due to β-PbO_2. (c) The X-ray powder diffraction pattern after 2 hr showing more comparable amounts of β-PbO_2 and Pb_3O_4. (d) The X-ray powder diffraction pattern after 4 hr showing only a small amount of the reactant, Pb_3O_4, remaining.

which is too short. Similar experiments were run at 0.1 and 0.05 N HNO_3 with the results shown in Table I. The half-times at 0.10 and at 0.05 are about 0.8 and 2.0 hr, respectively. From these experiments a concentration of 0.078 N was selected for the runs expected to be over in approximately 4 hr. The detailed results reported here are from these experiments. The weighted average of four runs for each time interval for the gravimetric measurements from the leaching experiments in 0.078 N HNO_3 are given in Table II.

The collection of micrographs that is Figs. 3a–3e shows the progress of the overall leaching process. In Fig. 3a the original

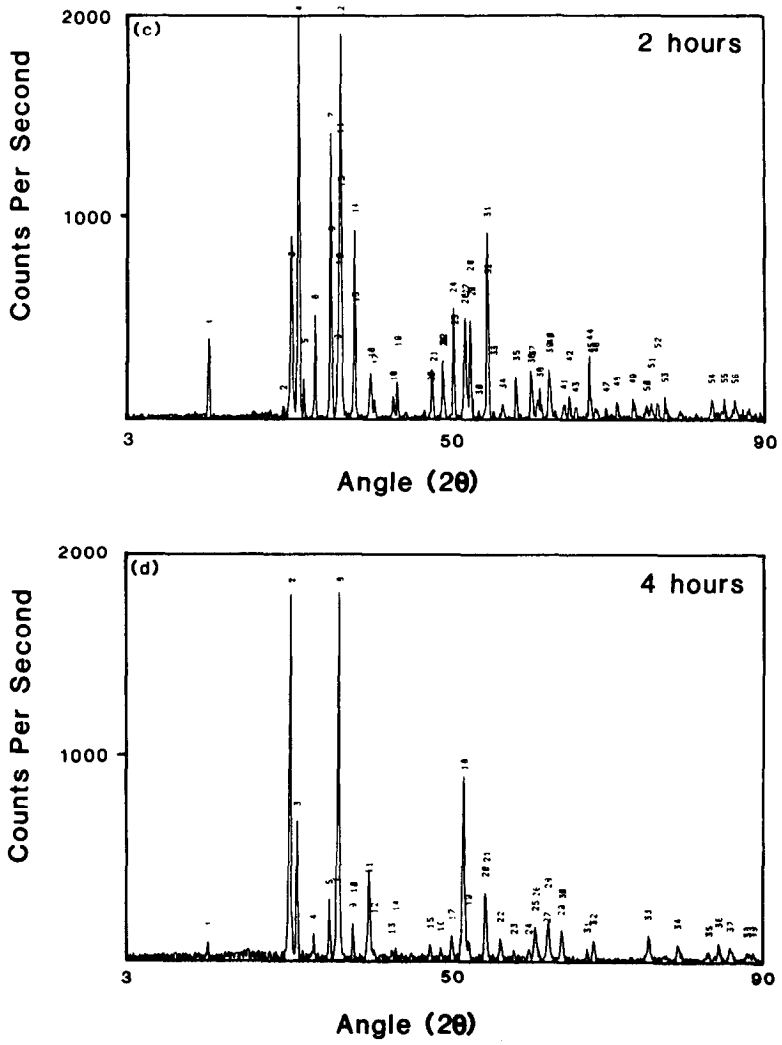

FIG. 2—*Continued.*

material is shown to consist of a collection of small particles of Pb_3O_4 of about 500–1000 nm in diameter. In Fig. 3b the deposition of PbO_2 after $\frac{1}{2}$ hr of reaction is shown to be distributed over the entire surface of the original crystal to an average shell thickness of about 30 nm. After 1 hr the reaction surface has decreased with the shrinking radius as shown in Fig. 3c. The surface shell of PbO_2 has thickened to about 50 nm. At 2 hr it had increased to about 85 nm thick. After 4 hr the reaction is essentially complete and the recrystallization is well underway. Notice, for example, the needle-like crystals projecting out from the mass as well as the appearance of well-faceted small crystals. After 8 hr, as shown in Fig. 3d, only β-PbO_2 (or its modification discussed in a separate publication) remains as well-articulated crystals unassociated with the original Pb_3O_4 particle that reacted at a continually receding surface until

TABLE I

OBSERVATIONS ON THE RATES OF LEACHING Pb_3O_4 BY HNO_3 AND CH_3COOH AT ROOM TEMPERATURE

Time (hr)	Fraction reacted (α)
In 0.1 *N* HNO_3 (25 ml)	
0.50	0.51
1.0	0.77
1.5	0.83
2.0	0.93
2.5	1.0
3.0	1.0
In 0.05 *N* HNO_3 (50 ml)	
0.50	0.063
0.93	0.202
1.50	0.450
1.93	0.516
4.47	0.636
2.93	0.732
3.42	0.895
In 10% CH_3COOH (25 ml)	
0.5	0.88
1.0	1.00

Note. In 1.0 *N* HNO_3 (25 ml) the reaction is over in less than 0.5 hr.

the reaction was complete. During and following the leaching there is relatively rapid recrystallization of the PbO_2 that grew from nuclei attached to the crystal surface and remained as electron conduits to the reaction surface.

The high-magnification image (Figs. 4a and 4b) gives a clear picture of the reacting surface after $\frac{1}{2}$ hr. The rough surface consists of grains of reacting Pb_3O_4 that can be identified at A by their scalloped edges and fringes. The PbO_2 crystals are, at this stage, rather rounded and highly disordered. After 1 hr the PbO_2 crystals have recrystallized into a disordered mass but notice, in Fig. 4c, the firm attachment of the crystals to the substrate. The needle-shaped crystals cover a range in length from about 6 to 12 nm.

Fig. 5 is a composite image at high resolution of a region of the reacting crystal shown in Fig. 4. On the right is a Pb_3O_4 crystalline domain arrested in its reaction after $\frac{1}{2}$ hr. The inserted patch on the left is the growing PbO_2 crystal. The composite is necessary since both regions could not be brought into focus and orientation at the same microscope settings but they do show the accurate juxtaposition of the spatially differentiated dissolution and precipitation centers. Optical diffraction pattern insets illustrate clearly the distinction between the order in the two structures. Notice the quite imperfect quality of the PbO_2 crystal including tilt twins and stacking faults. An amorphous region at (A) may well represent the earliest unstructured precipitation of PbO_2 that at a later stage was laid down in a more ordered fashion.

The optical diffraction patterns (ODP) are obtained from areas of 1 mm diameter on a negative produced at a magnification of 520,000× in the microscope. This means that this microoptical diffractogram is taken from an area of the crystal 2 nm in diameter. This diffractogram demonstrates a powerful method for obtaining confirmational evidence on the nature of different structures very close together as occur commonly in reacting systems in the solid state. The ODP from the ordered region near A indicates the rutile-type structure in the [100] direction with a c/a ratio of 1.46 and an angle between ⟨001⟩ and ⟨111⟩ of

TABLE II

THE LEACHING OF Pb_3O_4 WITH 25 ml OF 0.078 *N* HNO_3[a,b]

Time (hr)	Fraction reacted (α)	Fraction unreacted ($1-\alpha$)	$k't$ (Eq. (1))	$k''t$ (Eq. (2))	$\gamma C't$ (Eq. (3))
0.51	0.153	0.847	0.054	0.003	0.057
1.50	0.526	0.474	0.220	0.041	0.262
2.51	0.823	0.177	0.438	0.136	0.574
3.50	0.907	0.093	0.546	0.190	0.736
4.35	0.927	0.073	0.582	0.207	0.789
5.50	0.974	0.026	0.703	0.263	0.966

[a] The pH at the conclusion of each run is 1.36 ± 0.03.
[b] The temperature of the reaction is 28 ± 2°C.

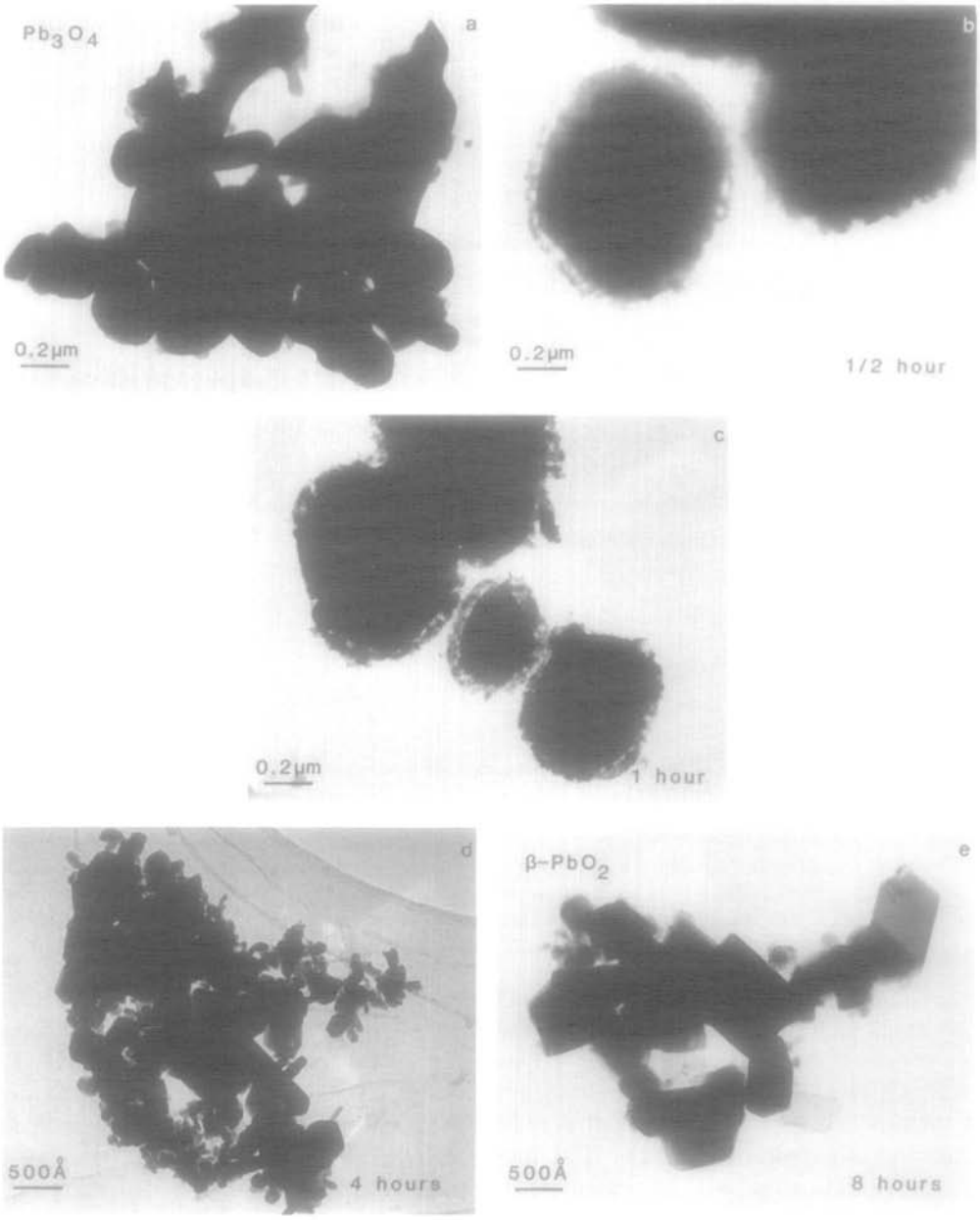

FIG. 3. (a) A high-magnification image of the starting material. Notice that it consists largely of chunky (spherical) particles about 1 μm in diameter. (b) An image of the Pb_3O_4 particles with their spongy crust of β-PbO_2 after $\frac{1}{2}$ hr of reaction. (c) The image of the reacting system after 1 hr. Notice the increase in the thickness of the precipitated PbO_2. (d) An image after 4 hr showing the β-PbO_2, now largely recrystallized, with only a small fraction of the Pb_3O_4 unreacted. (e) An image of the recrystallized β-PbO_2 after 8 hr when the leaching reaction is complete.

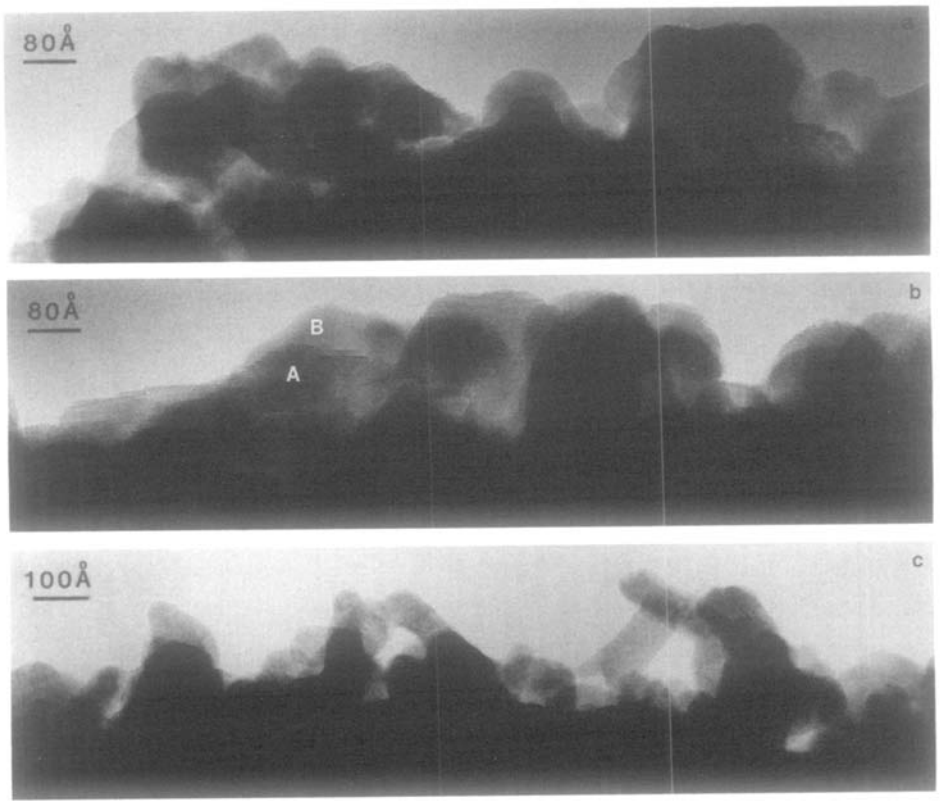

FIG. 4. (a,b) Images of the reacting surface of Pb_3O_4 after $\frac{1}{2}$ hr. Notice the mixture of reacting grains of Pb_3O_4 with their sculptured faces as at A and rather globular growing crystals of β-PbO_2 at B. (c) The image of a reacting crystal after 1 hr shows the development of the thatch of interconnected crystals of β-PbO_2 that leave room for the ionic diffusion required to permit the reaction to continue. These needle-like crystals rooted on the Pb_3O_4 surface maintain electrical contact as the interlinked sponge continues to grow.

55.6° as expected from β-PbO_2. The ODP from region B is from the ⟨010⟩ orientation of a Pb_3O_4 crystal. The ratio of the reciprocal vectors c/a is 1.37 (1.34 from ASTM cards) and the angle between the ⟨100⟩ and the ⟨101⟩ directions is 53° (53.3° calculated). The scalloped surface profile along the thin {101} edge reveals the progress of the reaction quenched during the process.

After 1 hr the reaction has proceeded to the point of showing developed projections of the growing and recrystallizing PbO_2 crystals as seen in Fig. 6. In Fig. 6 one observes a growing PbO_2 crystal with extensive defects; perhaps it is even polycrystalline. This crystal is attached at its base to the Pb_3O_4 reactant and probably is grown from the dissolving material forming the depression on either side. The protruding PbO_2 crystal shown in Fig. 7 is generally more perfect but a modified structure is apparent at its growing tip and many stacking faults still remain.

In Fig. 8 an image of a PbO_2 crystal after 8 hr of growth and recrystallization shows a rather well-formed β-PbO_2 core in the [100] orientation with a new structure, most apparent at the tip, and as an overall moiré pattern. The new structure will be discussed elsewhere.

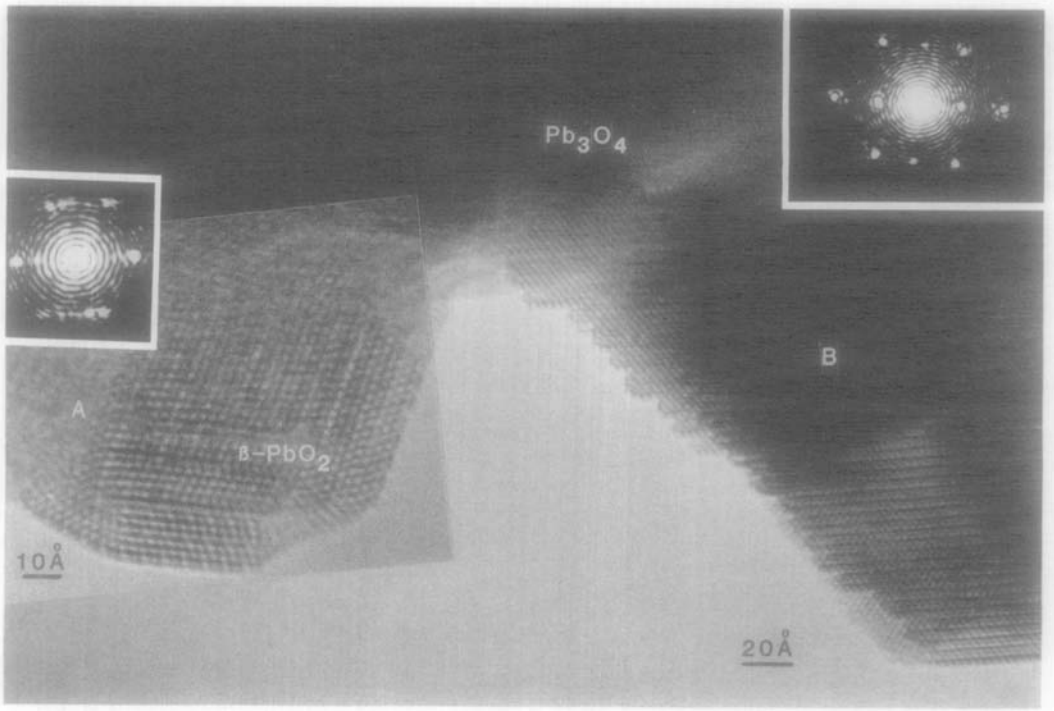

FIG. 5. A composite, high-resolution micrograph showing the details of disproportionation solution at B and the deposition recrystallization at A. Notice evidence of rapid reaction on the {101} face with its scalloped edge while no apparent reaction takes place on the {100} faces. The β-PbO_2 crystal at A grows at the expense of the dissolving substrate. The image maintains the spatial relationship of dissolution and deposition. It is a composite because it was not possible to image both regions simultaneously with the same microscope settings of focus and tilt.

Discussion

The solvolytic disproportionation of Pb_3O_4 has been studied by chemical, X-ray, and electron microscopic means. The X-ray patterns could be interpreted entirely as the growth of β-PbO_2 into Pb_3O_4 as a function of time until only PbO_2 remained. The chemical studies provided information on the macroscopic kinetics of the reaction by revealing the relative amounts of the two materials as a function of time. The electron microscopic results are consistent with the X-ray and chemical results and together these studies allow a detailed mechanism to be proposed.

The Gross Kinetics

Wadsworth (*11*) describes the derivation of a rate law that would apply to a homogeneous spherical particle undergoing leaching while forming a reaction product on the surface. The model assumes chemical attack on a homogeneous spherical particle forming a porous layer of solid reaction products on its surface. The kinetics are controlled by both the rate of reaction at the receding spherical surface of the particle and the rate of transport of Pb^{2+}(aq) to the nucleated product layer between the reaction zone and the outer periphery of the particle. This model is based upon steady-

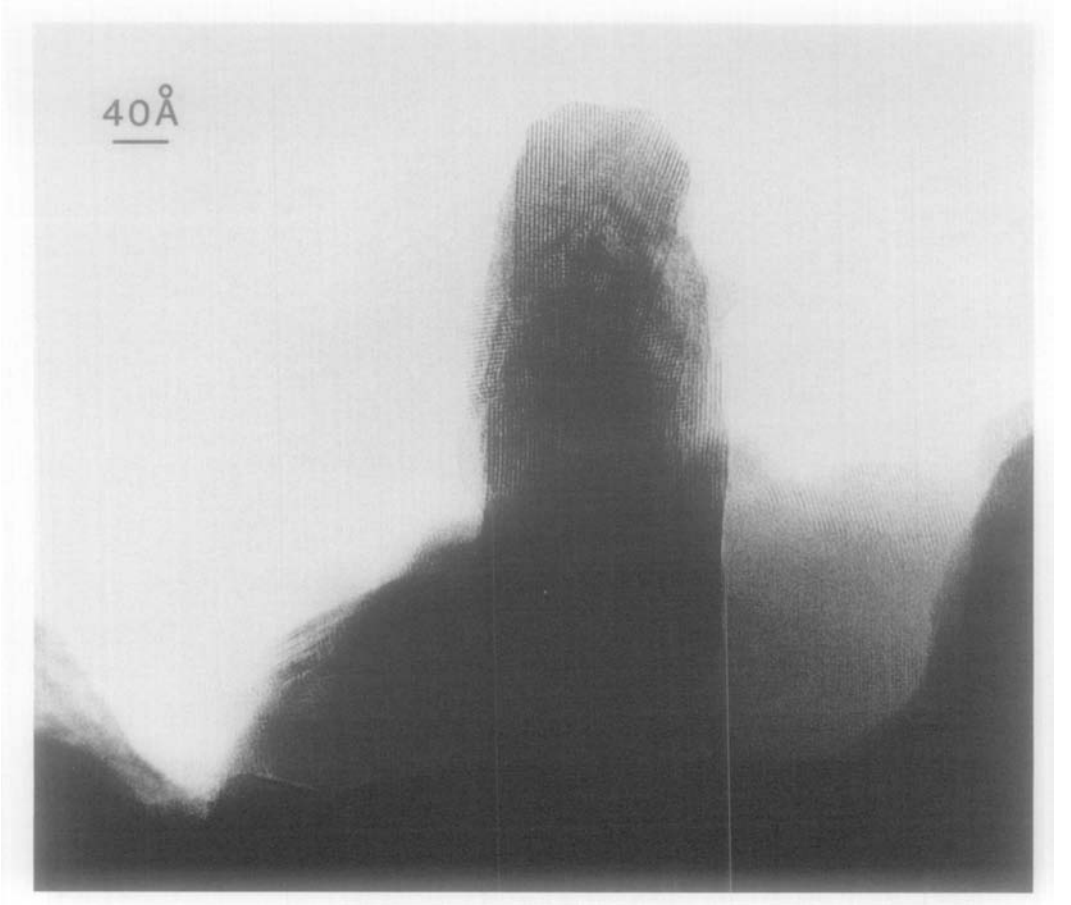

FIG. 6. An image illustrating the growth habit of the precipitating crystal. The principal growth direction is ⟨011⟩ but the crystal is clearly faulted.

state conditions in which the rate of diffusion of $Pb^{2+}(aq)$ through the pores in the shell outside the reaction zone equals the rate of leaching at the reaction zone. Diffusion of $H^{+}(aq)$ to the reaction zone is not rate controlling. The rate laws given are

$$[1 - (1 - \alpha)^{1/3}] = k_o' t, \qquad (1)$$

where α = the fraction reacted, k_o' is a constant, and t = time, for reaction on a sphere of decreasing radius, and

$$1 - \tfrac{2}{3}\alpha - (1 - \alpha)^{2/3} = k_o'' t, \qquad (2)$$

where k_o'' is a constant, for the transport of solvent through the growing product layer. The combined rate law is

$$1 - \tfrac{2}{3}\alpha - (1 - \alpha)^{2/3} + \beta[1 - (1 - \alpha)^{1/3}] = \gamma C t. \qquad (3)$$

In this expression β and γ are complex constants that cannot accurately be evaluated in this case. Results of the calculations of Eq. (1), (2), and (3) are given in Table II. (The constant β in Eq. (3) is taken to be one.) Although the scatter in the results from the kinetic measurements is so large that a quantitative treatment is not profitable, the relatively better fit to Eq. (3) than for either Eq. (1) or Eq. (2) is not inconsis-

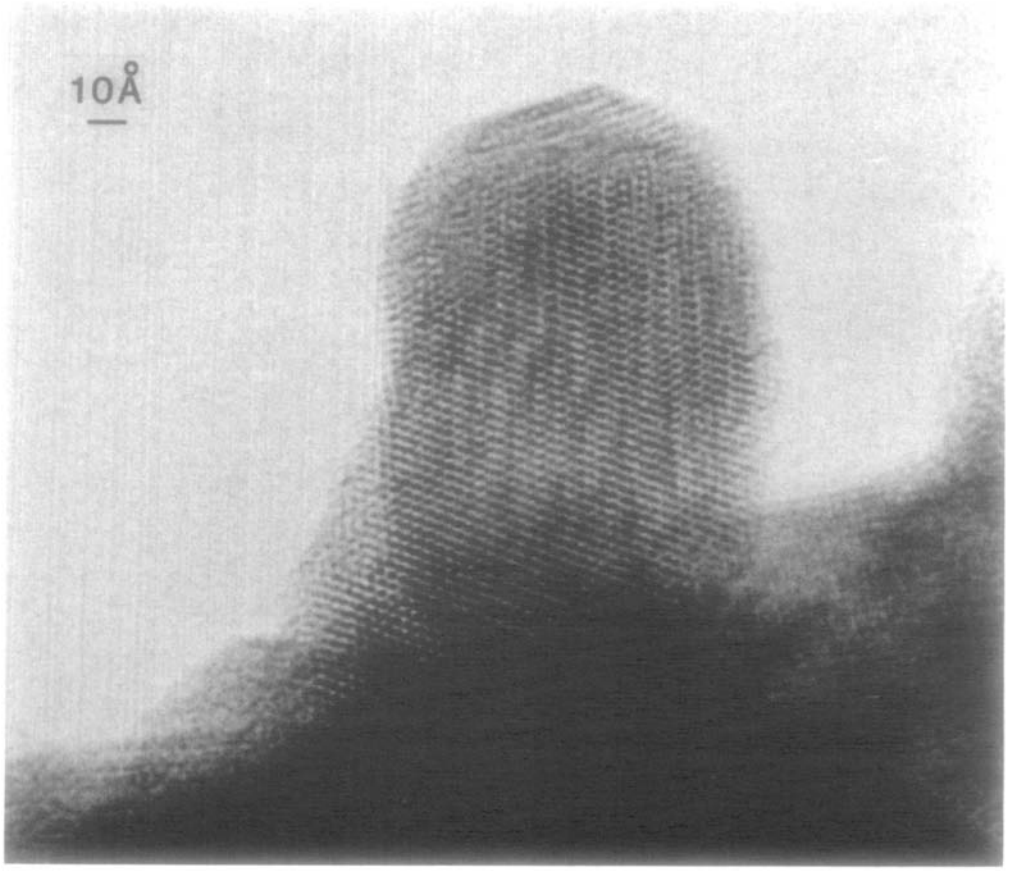

FIG. 7. The image of a growing crystal of β-PbO_2 in which there is disorder from stacking faults but no twin or tilt boundaries. Notice, however, the appearance of a different crystalline form at the tip. The principal axis of the crystal is [011].

tent with the mechanism proposed below on the basis of high-resolution electron microscopic observations. The reason for the scatter is most probably attributable to an absence of temperature control with a variable excursion of temperature of a few degrees depending on the stirring system used.

The Reaction Mechanism at the Atomic Scale

The details in the HREM images (Fig. 5) of Pb_3O_4(s) at various stages of dissolution enable an atomic-scale mechanism for the dissolution and subsequent PbO_2 microcrystallite formation process to be proposed. It is well known that dilute HNO_3(aq) dissolves PbO(s) according to the following equation:

$$PbO(s) + 2H^+(aq) = Pb^{2+}(aq) + H_2O. \quad (4)$$

On the other hand, PbO_2(s) is relatively insoluble in dilute HNO_3 (*12*). The data of Hara (Fig. 9) illustrate the solubility differences well (*13*). Lead solubility data for both PbO(s) and PbO_2(s) maintained in contact with agitated HNO_3 solutions of various strengths for 1 hr are reported and PbO is approximately 5×10^3 times more soluble

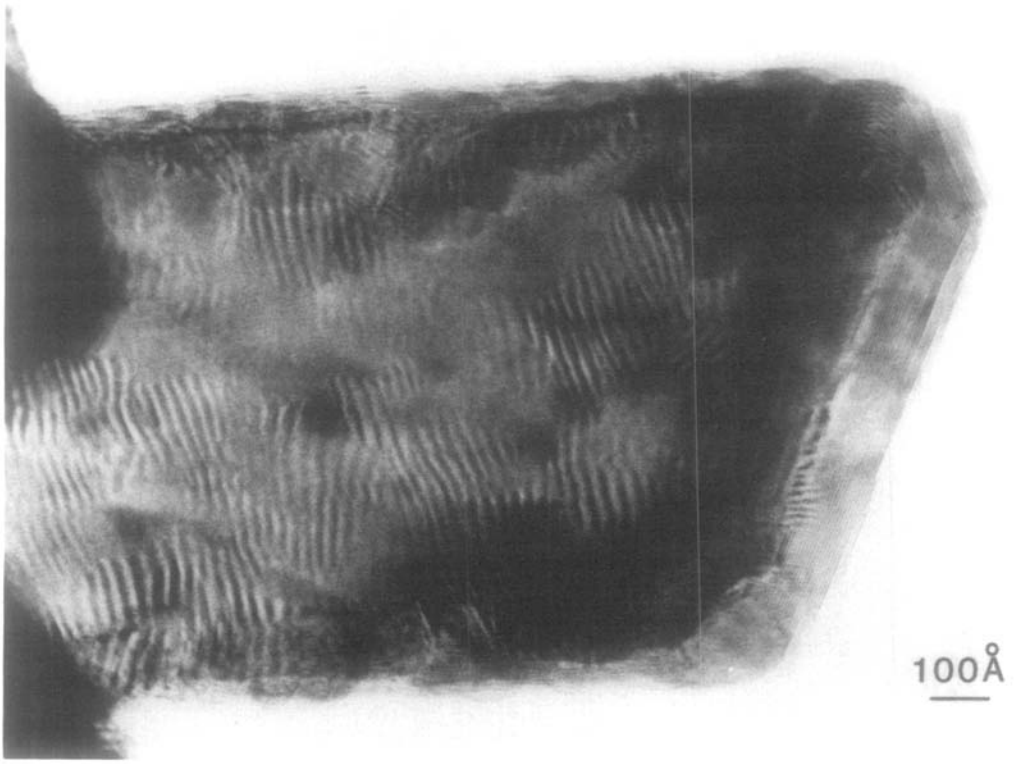

FIG. 8. The image of a fully developed crystal of β-PbO_2 that has an envelope of a modified structure. The moiré pattern over the surface is probably due to the overburden of "modified" β-PbO_2 that covers the surface.

than PbO_2(s) in 1 *N* solutions. PbO_2 dissolution occurs with reduction of the lead according so the reaction (*14*)

$$PbO_2(s) + 2HNO_3 \rightarrow Pb(NO_3)_2 + H_2O + O_2. \quad (5)$$

Solid Pb_3O_4 is composed of octahedrally coordinated Pb^{4+} ions joined together by Pb^{2+} ions which are nestled in a distorted tetrahedron of oxygen ions (*6–8*). Figure 10 illustrates the structure of Pb_3O_4. The octahedra share edges to form chains which run parallel to the *c*-axis [001], and share apices in {110}. Two joined octahedra constitute the *c*-axis. The Pb^{2+} ions are located on {110} planes, while Pb^{4+} ions are situated along the {010}, {100}, {020}, and {200} planes. When the Pb_3O_4 structure is viewed along {100}, the octahedra edge-shared along *c* appear unconnected in rows parallel to *b*. Another octahedral row displaced rearward by 0.5 *b* and offset by 0.5 *a* lies immediately behind every row.

From the [010] image (Fig. 5) it can be deduced that to a first approximation dissolution occurs principally along {101}, and secondarily along {001}, with minimal dissolution along {100}. Other images are consistent with that presented in Fig. 5; the principal plane of dissolution usually makes an angle of ~127° with a plane at which minimal dissolution occurs, consistent with the calculated interplanar angle of 53.1° between {100} and {101}. Along the edge of (101), the dissolution plane, sharp points of

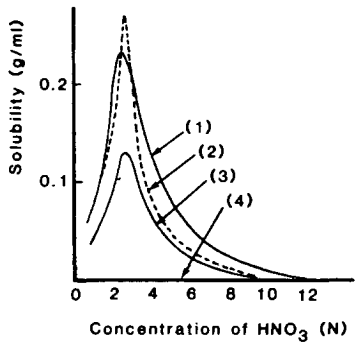

FIG. 9. A plot of the solubilities of lead and its oxides as a function of the concentration of nitric acid (from Hara (*13*)).

contrast protrude from regions that appear rounded, but are probably composed of {100}, {101} and {001} faces.

The proposed mechanism involves acid dissolution of the Pb^{2+} ions which are exposed in the {001} faces at the termini of the PbO_2 octahedral chains. Attack occurs between the chains along {110} and {001} according to the reaction:

$$Pb_3O_4(c) + 4H^+(aq) = PbO_2(s) + 2Pb^{2+}(aq) + 2H_2O. \quad (6)$$

Removal of the Pb^{2+} ions that hold the chains together as well as some of their associated oxygen ions allows the octahedral chains at the edge of the crystal to break loose. In order to dissolve, the Pb^{4+} atoms in this "released" part of the chain must next be reduced to the divalent state according to the following equation:

$$PbO_2(s) + 2e^-(s) + 4H^+(aq) = Pb^{2+}(aq) + 2H_2O(1). \quad (7)$$

This dissolution process is discussed later. Loss of the "PbO" means that the Pb^{4+} ion can no longer be sheathed by six oxide ions. Either its oxygen coordination must decrease to four and the Pb^{4+} ions must assume tetrahedral coordination or oxygen atoms from water molecules must complete the coordination sphere. Either way, this

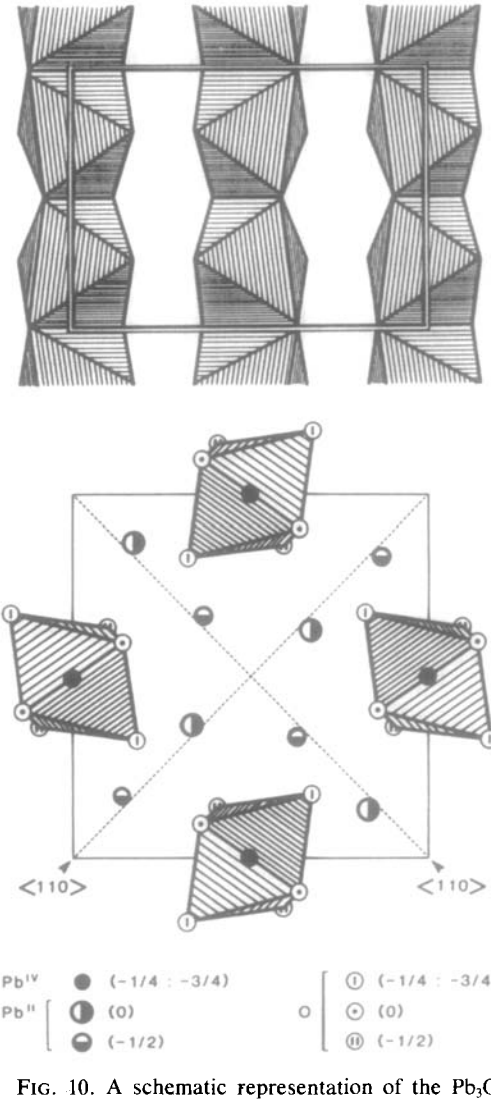

FIG. 10. A schematic representation of the Pb_3O_4 structure; *ab* projection at bottom, *a,c* elevation (viewed upward from the *ab* projection) at the top. The strings of shaded octahedra containing Pb(IV) share edges along *c* while the Pb(II) are deployed in the {110} planes. In the *ac* elevation shown the Pb(II) are eclipsed, thus attack on PbO must occur along ⟨110⟩ to release the Pb(IV) columns that are then vulnerable to reduction and dissolution.

Pb^{4+} ion is vulnerable and susceptible to reduction. Loss of a PbO_2 "octahedron" exposes the octahedron behind it to attack along {110}, allowing the dissolution process to continue. Thus, dissolution occurs with individual PbO_2 "octahedra" being removed and, in the process, exposing octahedra which lie deeper in the fragment for subsequent removal. Since the unit cell is tetragonal, dissolution can also occur on faces perpendicular to that observed in Fig. 5. This dissolution process ensures that if the dissolving fragment is wedge-shaped it remains wedge-shaped. A spherical particle, on the other hand, can only have dissolution occur at its exposed surface and need not become wedge-shaped. The sharp points of contrast that protrude from the edge of the dissolution plane may imply that instead of individual "octahedra," a row of "octahedra" breaks loose simultaneously, but, of course, remains attached to the dissolving particle until each Pb^{4+} ion has been reduced. A row of ions could share oxygen atoms more advantageously and retain a higher coordination number than could a single ion.

Reduction of the Pb^{4+} ion would appear to be a slow step in the dissolution process. Since PbO_2 is relatively insoluble in dilute HNO_3, the PbO_2 chains can either break off and be removed from the reaction area, or can dissolve by a redox process. The rapid growth of rigidly attached microcrystallites supports a redox mechanism. (There is no evidence of the extremely small particles consisting of associated (octahedrally coordinated) chains that would pass through the filter and give low gravimetric results.)

The proposed mechanism requires the presence of Pb^{2+}(aq) ions. These ions can come initially from two sources. The first and principal source involves selective dissolution of the Pb^{2+} ions from the crystal edge. The excursions apparent in Fig. 5 at the dissolving edge probably result from this initial selective dissolution process and, once formed, persist. The second source is the Pb^{4+} left after the Pb^{2+} "glue" has been removed. These Pb^{4+} ions can dissolve according to Eq. (5) by being reduced to Pb^{2+} with concomitant liberation of oxygen.

For a redox mechanism to operate, electron transport must take place through the solid, whereas Pb^{2+} ion transfer occurs through the solution. The specific conductances of Pb_3O_4 and PbO_2 are 4.3×10^{-11} and 2.48 Ω^{-1} cm^{-1}, respectively (*15*, *16*) thus PbO_2 can readily support electron transfer. However, Pb_3O_4(s) is reported to be a p-type semiconductor (*15*). In PbO_2 all Pb^{4+} ions are octahedrally coordinated with the chains of octahedra formed by sharing oxygen ions. It is proposed that electron transfer occurs through the octahedra left after the Pb^{2+} ions are dissolved such that Pb^{2+} ions precipitate from solution as PbO_2 onto a crystal face close to that of the dissolving face according to the reaction,

$$Pb^{2+}(aq) + 2H_2O(l) = PbO_2(s) + 4H^+(aq) + 2e^-(s). \quad (8)$$

As these Pb^{2+} ions are oxidized on the surface of the growing crystal to Pb^{4+}, electron transfer occurs through the fragment to reduce an "octahedral" Pb^{4+} ion either in the (101) face, or more likely, already being released from the face, thereby allowing it to become solvated as a Pb^{2+} ion according to reaction (7). These Pb^{2+} ions then diffuse through the solution across a concentration gradient to the growing crystallite. Oxide ions necessary for lead dioxide growth come from the solvent. The rapid growth of the crystal of PbO_2(s), evidenced by the disorder apparent in the image, is an indication of the speed with which electron transfer can occur. The PbO_2 microcrystallites recrystallize continuously as reversible precipitation reaction (8) takes place. In this recrystallization process both transport and exchange occur.

The proposed mechanism is consistent with {101} being the face from which dissolution occurs most rapidly. In the proposed dissolution process a particle initially would have a jogged (001) face at which the octahedral chains of PbO_2 terminate. Dissolution initiates at this (001) face, making excursions into it (parallel to c) and simultaneously dissolving Pb^{2+} along {110} at the edge of the particle. The Pb^{4+} octahedron at the edge breaks loose from the main body of the crystal and dissolves, as described above, creating a step at the surface of the particle. Attack now takes place in the same manner, removing the row immediately below that which was just removed, and simultaneously removing the row behind the one just removed. Since the Pb^{4+} ions are centered at 0.25 and 0.75 along z, a (101) face has been created and will propagate as row after row of octahedra are removed.

As the particle becomes wedge-shaped some areas near the edge will become thinned and will erode through. Such erosion would also appear as indentations in the (001) face, and is apparent in Fig. 5, but the principal thrust of the dissolution process remains (101) with (001) secondary.

Why should crystallite growth occur? Clearly, lattice energy alone would dictate that even disordered PbO_2(s) in a microcrystal is more stable (i.e., of lower energy) than is PbO_2(s) in a shred left by dissolution of the surrounding Pb^{2+} and associated oxide ions. Furthermore, PbO_2(s) is known to be reduced rapidly by both the one- and two-electron reducing agents, Cr^{2+} and U^{4+} (*17*, *18*). From radiotracer exchange reaction studies, Pb^{2+}(aq) and PbO_2(s) are known to undergo exchange rapidly (*19*), with the rate of exchange being very dependent upon the surface condition of the PbO_2(s). Freshly prepared PbO_2(s) has been reported and subsequently confirmed to undergo rapid exchange with Pb^{2+}(aq), equivalent to an amount equal to 10 to 20 atomic layers of the solid (*19*, *20*). Such rapid exchange is reported to be irreproducible and to decrease with aging of the PbO_2.

The HREM data and the exchange mechanism proposed for the Pb_3O_4 selective solvation process indicate both why the exchange is irreproducible and why it decreased with aging. In the exchange reactions freshly precipitated PbO_2(s) was in contact with $*Pb^{2+}$. The environment was comparable to that present in the "leaching" experiment. Initially rapid exchange occurred, with PbO_2(s) on faces unfavorable to growth dissolving and $*Pb^{2+}$ oxidizing and precipitating on faces which exhibit favorable growth characteristics. With time, the PbO_2(s) was converted to PbO_2 microcrystallites. Initially, of course, a higher ratio of $*Pb^{2+}$ precipitated, but as nonradioactive Pb dissolved and equilibrated, a solution progressively more rich in the latter substance developed, and a steady state of precipitation resulted. This hypothesis effectively explains the irreproducible observations of Bone *et al.* (*19*).

In summary, one of the driving forces of the reaction appears to be the minimization of surface energy and development of lattice energy. This minimization can be achieved most efficiently by a redox-solution-precipitation mechanism. This mechanism would seem to be applicable only in a specimen which:

(a) is an electrical conductor to some degree,

(b) is capable of undergoing a redox reaction, and

(c) has one oxidation state which is soluble and one which is insoluble in the reaction medium.

Conclusions

The mechanism of solvolytic disproportionation is characteristic of the system involved and depends entirely upon the structures and chemical properties possessed by

the species and defects involved in the solid state and in the solution. It has been possible to put together an atomic-level mechanism from the examination, in the high-resolution electron microscope, of the reacting solid-state system, quenched as the reaction progressed. The mechanism for the solvolytic disproportionation of Pb_3O_4 can be summarized as follows.

1. Dilute HNO_3 attacks the clean surface of polycrystalline Pb_3O_4 leaching out the Pb^{2+} according to the reaction

$$Pb_3O_4(s) + 4H^+(aq) = PbO_2(s) + 2Pb^{2+}(aq) + 2H_2O(1) \quad (6)$$

and the concentration of $Pb^{2+}(aq)$ begins to rise.

2. Two coordinated processes then begin, necessarily simultaneously. The $PbO_2(s)$ formed in reaction (6) is highly reactive since it is produced incompletely coordinated at the surface of the Pb_3O_4 crystal and in particles of molecular size. This instability results in the solution of PbO_2 according to

$$PbO_2(s) + 2e^-(s) + 4H^+(aq) = Pb^{2+}(aq) + 2H_2O(1) \quad (7)$$

accompanied by the precipitation of Pb^{2+} at a nearby site where a crystal of PbO_2 is nucleating or growing. This latter reaction is Eq. (7) in reverse. The driving force is the free energy difference between molecular-sized species containing Pb^{4+} and a reasonably well-crystalized PbO_2. Diffusion of $Pb^{2+}(aq)$ through the solution accomplishes the mass transport necessary. The electrons, transported through the solid, complete the circuit.

Still another reaction occurs concurrently. The imperfect crystals first precipitated grow at a reasonably fast rate to form more perfect crystals with certain preferred facets and growth directions (needles along ⟨011⟩ with (010) and (001) facets). This is accomplished by the rapid exchange represented again by the reversible eq. (6).

This mechanism results from (1) a structure from which one fraction cannot be removed without leaving the other normally impervious fraction vulnerable to disintegration, and (2) a system consisting of a rapidly reversible pair, Pb^{2+} (aq) and Pb^{4+} (s), that preserves a relatively clean reactive surface and removes the otherwise inhibiting solid product to another site. The product forms an interconnecting porous crust around the reactant that assures the necessary electron conduction required for the reaction to go to completion without throttling it. The overall rate law followed is consistent with these atomic-level observations.

Acknowledgments

We are grateful to the NSF for support through Research Grant DMR-8516381 and the HREM facility grant DMR-8306501. We acknowledge with thanks the help of Dr. Ann Yates in obtaining the X-ray diffraction patterns.

References

1. A. F. Clifford, *in* "Rare Earth Research II" (K. S. Vorres, Ed.), pp. 45–50, Gordon & Breach, New York (1963).
2. Z. C. Kang and L. Eyring, *J. Solid State Chem.* **75,** 52 (1988).
3. Z. C. Kang and L. Eyring, *J. Solid State Chem.* **75,** 60 (1988).
4. C. Brückner, *Chem.-Ztg.* **51,** 55 (1927).
5. J. C. Bailar, *in* "Comprehensive Inorganic Chemistry" (A. F. Trotman-Dickenson, Ed.), Vol. 2, pp. 120, Compendium Publishers, Elmsford, NJ (1973).
6. S. T. Gross, *J. Amer. Chem. Soc.* **65,** 1107 (1943).
7. M. K. Fayek and J. Leciejewicz, *Z. Anorg. Allg. Chem.* **336,** 104 (1965).
8. S. R. Cavarri and D. Weigel, *J. Solid State Chem.* **13,** 252 (1975).
9. J. Leciejewicz and I. Padlo, *Naturwissenschaften* **49,** 373 (1962).
10. S. Iijima, *Acta Crystallogr. Sect. A* **29,** 18 (1973).
11. M. E. Wadsworth, *in* "Physical Chemistry: An Advanced Treatise" (H. Eyring, D. Henderson, and W. Jost, Eds.), pp. 413–470, Academic Press, New York (1975).

12. "Handbook of Chemistry and Physics" (R. C. Weast, Ed.), p. B107, CRC Press, Boca Raton (1985).

13. N. HARA, *Ind. Health* **5,** 60 (1967).

14. N. N. GREENWOOD AND A. EARNSHAW, "Chemistry of the Elements," pp. 449, Pergamon, Oxford (1985).

15. A. V. PAMFILOV, E. G. IVANCHEVA, AND P. V. DROGOMIRETSKII, *Zh. Fiz. Khim.* **41,** 1072 (1967); *Chem. Ab.* **67,** 77,061m (1967).

16. J. HEMPOELMANN, *Naturwissenschaften* **62,** 343 (1975).

17. G. GORDON AND H. TAUBE, *Inorg. Chem.* **1,** 69 (1962).

18. B. A. ZABIN AND H. TAUBE, *Inorg. Chem.* **3,** 963 (1964).

19. S. J. BONE, M. FLEISHMANN, AND W. F. K. WYNNE-JONES, *Trans. Faraday Soc.* **55,** 1783 (1959).

20. B. PULLMAN AND M. HAISSINSKY, *J. Phys. Radium* **8,** 36 (1947).